Batteries & Supercaps

Research Article
doi.org/10.1002/batt.202400394

Chemistry Europe
European Chemical Societies Publishing

www.batteries-supercaps.org

# Experimental Set-Up for Measurement of Half-Cell- and Over-Potentials of Flow Batteries During Operation

Gabriel Gonzalez[a] and Pekka Peljo*[a, b]

The study of flow batteries (FBs) requires the development of tools able to evaluate their performance during operation in a reliable and simple way. In this work, we present an experimental set-up that allows the on-line monitoring of the half-cells state of charge and apparent overpotentials on the positive and negative electrodes during battery operation. These measurements are feasible by using additional flow cells that include a reference electrode on each side. We used the experimental set-up to study the performance of the vanadium system as well as a previously reported stable organic couple. The studies consisted on short cycling operation at different current densities and polarization curves at different flow rates and states of charge. By confirming previous results obtained for vanadium-FBs and extending the analysis to further systems, we demonstrated that this approach provides a reliable deeper insight into the battery performance and the processes taking place during operation.

## Introduction

In the last decades, Flow Batteries (FBs) have become a promising large-scale energy storage alternative to solve the imbalance between consumption and production from renewable sources.[1,2] They offer long cycle life and fast response time, coupled with their unique ability to size energy and power separately: stored energy capacity is defined by the volume of the tanks while the power output by the numbers of cells on the stack. That makes FB technology a scalable and flexible energy storage system. The most developed FB technology utilizes vanadium electrolyte, and vanadium-FBs are currently being commercialized.[3] Because of the high volatility of the vanadium price, relatively low energy density and low annual vanadium production, plenty of research is focusing on the development of alternative chemistries to replace vanadium as the active material.[4] Aqueous Organic FBs (AO-FBs) consisting on organic redox molecules present major advantages because of their tunability, scalability and potential low cost. Up to date, viologens, quinones and nitroxyl radicals, among others, have been reported with promising results.[5] The drawbacks of the organic materials are mostly related with their lower stability and solubility, which leads to lower lifespan and energy density compared with the vanadium technology.

One of the main challenges on the development of the FBs is the capacity decay during operation, which is mainly attributed to crossover of species through the membrane, decomposition of the active material and side reactions such as oxygen evolution reaction (OER) or hydrogen evolution reactions (HER). These processes can lead to either irreversible or reversible capacity decay on the cell by limiting one of the sides and leading to a cell imbalance. In the case of vanadium, its chemistry offers high stability besides four oxidation states that allow having the same electrolyte on both sides of the cell, enabling the rebalancing of the electrolyte by simple mixing processes.[6] However, this become a further problem for organic systems as the active molecules are more susceptible to chemical decomposition leading to irreversible capacity losses. The degradation mechanisms have been deeply studied,[7,8] which led to use molecular engineering to design new robust and stable molecules.[9] Up to date, broad improvements have been achieved on this sense, leading to highly stable aqueous organic systems.[10]

Both the development and proper control of these systems require identifying the processes occurring on the cell during operation, particularly those leading to capacity fade or to imbalance. Proper state of charge (SOC) monitoring allows better battery management, leading to improved battery performance.[11] More importantly, it allows prevention of problems arising from electrolyte imbalances, such as over-oxidation of the positive electrolyte leading to carbon corrosion and, in the worst case, to system failure.[12] During the development stage, a reliable on-line monitoring allows a deeper insight into the studied system, for example for comparison of different electrode and membrane materials, or evaluating the origin of the capacity fade or system imbalance. The monitoring of both sides of the cell separately allows detecting the limiting side and predicting the cause of fade. On this sense, many methods have been reported to measure the individual half-

[a] G. Gonzalez, Prof. P. Peljo
Research group of Battery Materials and Technologies, Department of Mechanical and Materials Engineering, University of Turku, Quantuminkuja 1, 20014 Turku, Finland
E-mail: pekka.peljo@utu.fi

[b] Prof. P. Peljo
Department of Chemistry and Materials Science, Aalto University, Kemistintie 1, 02150 Espoo, Finland

Supporting information for this article is available on the WWW under https://doi.org/10.1002/batt.202400394

cells state of charge (SOC) of the cell.[6,13] The most popular approach consists on measuring the half-cells potential against a reference electrode. Some studies performed the on-line measurement externally by using a reference and a carbon electrode immersed in the reservoirs,[14] in a custom made flow armature after the cell,[15] or using additional flow cells that have the electrodes incorporated.[16] Other works integrated the reference electrodes into the main cell using dynamic,[17,18] or through-plate reference hydrogen electrodes that were previously applied for fuel cells evaluation.[19] Otherwise, the monitoring of the individual half-cells SOC of vanadium-FB has also been conducted by measuring physical properties of the electrolyte, as density, viscosity, conductivity and absorbance.[6,13] The cited techniques have been mostly restricted to analyze the vanadium system, while little research has focused on studying the performance of the other flow battery chemistries.

Besides the study of the half-cells SOCs, the measurement of electrode overpotentials can provide crucial information for optimization of the cell performance and its components.[20] The potential losses due to concentration or kinetic effects can lead to low battery efficiency and capacity utilization. The study of the flow cells overpotentials on vanadium-FBs has been conducted using polarization curves[21] and impedance techniques.[22] However, these techniques are limited to a particular time of the battery so they cannot be used for online monitoring during operation. Furthermore, the polarization curves study does not provide information about the individual half-cells and how the potential losses are distributed on each side of the battery. Roth et al.[23] solved this limitation by inserting two reference electrodes as Lugging capillaries on each side of a vanadium battery and determined the individual electrode polarization of each half-cell. Using a similar approach, Zago et al.[19] inserted through plate reference electrodes to study the electrodes polarization separately using both electrochemical impedance spectroscopy (EIS) and polarization curves. Their study confirmed the previous results reported for VFBs,[22–24] showing that most of the potential losses belong to the sluggish vanadium reactions on the negative electrode (activation overpotential) while mass transfer effects limit the positive electrode when applying higher current densities (concentration overpotential). However, while this work allowed to study the overpotentials of the half-cells separately, the measurements were conducted applying galvanostatic steps and calculating the overpotential as a difference between the potential when applying current and the open circuit potential (OCP) of each electrode. As such, they are not suitable for online overpotential monitoring during battery operation.

In this work, we present an experimental set-up that allows monitoring the half-cells state of charge and apparent overpotentials on the positive and negative electrodes during battery operation. Modification to access real overpotentials is also discussed. These measurements are performed by using additional flow cells assembled with the same carbon plate material and membrane as the main battery, while including a reference electrode on each side of the additional cell. In a previous work, we used a similar simplified configuration to study the performance of heat- and chemically- treated carbon felts working as positive and negative electrodes in a vanadium-FB.[25] In this work, we present the overall battery set-up as a powerful and reliable system that allows a deeper study of the battery performance and the processes involved during operation. We report and discuss the results obtained for the vanadium system and a stable organic couple reported by Aziz.[26] The studies consisted on short cycling experiments at different current densities and polarization curves at different flow rates and SOCs.

## Experimental Section

### Experimental Set-Up

The experimental set-up consists of two additional flow cells located before and after the battery. These cells are assembled with the same carbon plate material and membrane as the main battery; then, as the electrolyte flows through these cells and no current is flowing there, the open circuit voltage (OCV) can be measured before and after the battery during normal operation. This configuration also permits measuring the apparent overpotentials of both positive and negative electrodes separately by recording the potential difference between the end plates of the battery (polarized during operation) against the end plates of the additional cell (non-polarized). Unfortunately, this configuration results in some small shunt currents through both OCV-cells, resulting in offset in the measured apparent overpotential linearly scaled with the current. Furthermore, the cell after the battery comprises a leakless Ag/AgCl reference electrode (ET072 electrode from eDAQ) on each side that allows recording the half-cell potentials by measuring the potential of each carbon plate against the reference electrode. As the relationship between states of charge of the electrolytes and the redox potentials is known, the configuration allows recording the state of charge of the half-cells individually. Finally, we included the measurement of the potential drop through the membrane by measuring the potential difference between the reference electrodes located on each side of the OCV-cell after the main cell. A scheme of the experimental set-up including the measurements recorded during battery operation is depicted in Figure 1. Altogether eight different voltages are recorded during the flow battery operation:

1. Main cell voltage and current density.
2. Open circuit voltage (OCV) before the main cell.
3. Open circuit voltage (OCV) after the main cell.
4. Positive electrode half-cell state of charge (potential difference between positive electrode on OCV-cell against reference electrode Ag/AgCl).
5. Negative electrode half-cell state of charge (potential difference between negative electrode on OCV-cell against reference electrode Ag/AgCl).
6. Positive electrode apparent overpotential (potential difference between positive electrode on the main cell against the positive electrode on the OCV-cell).
7. Negative electrode apparent overpotential (potential difference between negative electrode on the main cell against the negative electrode on the OCV-cell).
8. Membrane potential drop (potential difference between the reference electrodes located on each side of the OCV-cell).

For recording real overpotentials, current flow through OCV-cell after the main cell has to be completely blocked. This was done by replacing membrane in OCV-cell after the main cell with a Teflon

Research Article
doi.org/10.1002/batt.202400394
Chemistry Europe
European Chemical Societies Publishing

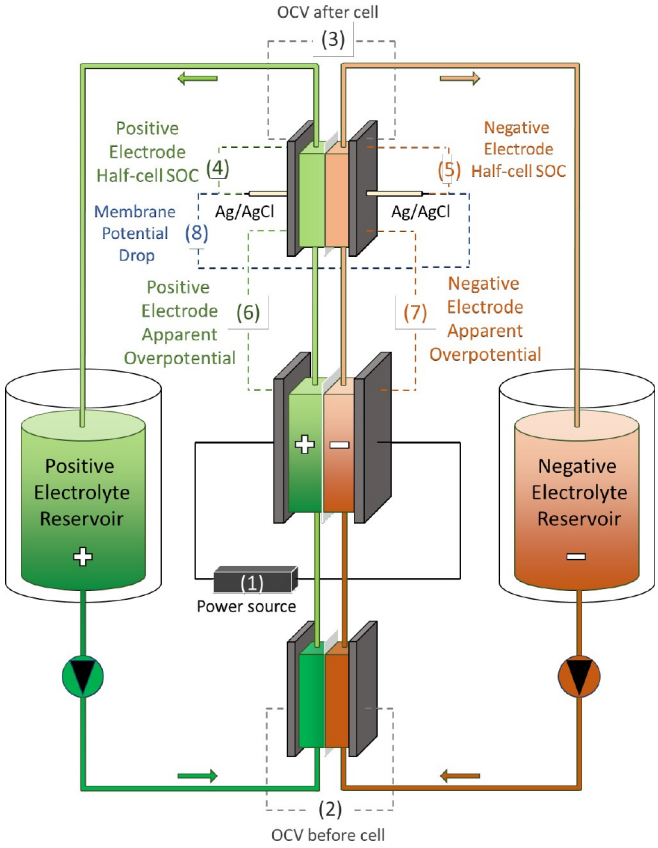


**Figure 1.** Experimental set-up including the measurements recorded during the experiments.

sheet, blocking the flow of the ionic shunt currents (Supporting information S7).

We recorded all the measurements using a LANHE Battery Testing System G340A (one channel for each measurement). In the case of the Vanadium System, we required additional channels in the main cell to apply the high currents needed for the polarization curves (max. current per channel: 5 amps). Additionally, we performed potentiostatic electrochemical impedance spectroscopy (PEIS) measurements to obtain the resistance of the main cell using a Biologic SP-240 potentiostat (see Supporting Information S6).

## Experimental Tests

We performed the studies using commercial Pinflow lab-scale cells. The main battery consists on a standard single cell with an active area of 20 $cm^2$ and a flow-through geometry. It was assembled using bipolar plates made of carbon-polymer composite, provided by Pinflow. The same material was used for the additional OCV-cells. The membrane and electrodes used for each system are presented in Table 1. The flow rate of the electrolyte was kept constant with a peristaltic pump (Baoding Chuangrui, with Masterflex C-Flex tubing). We performed charge-discharge curves and polarization curves at different conditions.

The charge-discharge curves consisted on short galvanostatic cycling using four different current densities (three cycles for each current value) with constant electrolyte flow rate of 100 mL $min^{-1}$. We measured the resistance of the system before and after each cycling experiment.

**Table 1.** Main characteristics and settings of the flow batteries studied.

| | Vanadium-FBs | | Organic-FB |
|---|---|---|---|
| Initial electrolyte composition | Positive and negative electrolytes: commercial vanadium electrolyte solution (1.6 M of vanadium in 2 M $H_2SO_4$) from GfE | | Positive side: 0.4 M BTMAP-Fc in 1 M KCl Negative side: 0.4 M BTMAP-Vi in 1 M KCl Commercial chemicals from TCI |
| Electrodes | VFB1 Rayon Graphite Felt BGF5 from CGT Carbon GmbH (heat-treated for 24 h at 400 °C) | VFB2 Thermally activated PAN carbon felts GFD 4.65 EA from SIGRACELL | Thermally activated PAN carbon felts GFD 4.65 EA from SIGRACELL |
| Exchange membrane | Nafion™ NR212 from IonPower | Selemion AMVN from AGC | Selemion AMVN from AGC |
| Cut-off voltages | +1.70 V/+0.90 V | | +1.00 V/ +0.40 V |
| Electrolyte degassing | Nitrogen gas bubbled to the reservoirs during the experiments | | Experiment conducted inside nitrogen-filled GloveBox |
| Electrolyte volume | 50 mL | | 40 mL |

The polarization curves were performed at three different states of charge (20, 50 and 80%) and three different flow rates (20, 50 and 100 mL $min^{-1}$). First, the curves were performed using the standard slope approach (increasing of the current: 5 A/60 s) during discharge. Additionally, we conducted the experiments in galvanostatic mode using current steps of 30 seconds and measuring the cell voltage at the steady state, followed by a resting time at the open circuit voltage. Each discharging step was alternated with a charging step with the same current in order to keep the state of charge of the reservoirs constant. The discharge and charge current values were gradually increased on each step until the battery voltage was 0 V and the upper cut-off voltage of the system, respectively. The voltage measured in each step corresponds to a point of the polarization curve. This method allows the measurement of the polarization curve without changing the state of charge of the cell during the experiment[27] and we used it to compare the results with the standard slope approach. We measured the resistance of the system before and after each polarization curve.

## Studied Systems

During this work, we used the described battery set-up to study the performance of the vanadium-FB and a stable organic couple consisted on a bis((3-trimethylammonio)propyl)-ferrocene dichloride (BTMAP-Fc) as positive electrolyte and bis(3-trimethylammonio)propyl viologen tetrachloride (BTMAP-Vi) as negative electrolyte. In the case of Vanadium, we include the study of two systems using different treated carbon felts as electrodes to analyze their influence on the apparent cell overpotentials. The main characteristics and settings of the studied systems are summarized in Table 1.

Research Article
doi.org/10.1002/batt.202400394
Chemistry Europe
European Chemical Societies Publishing

## Results and Discussion

### Charge-discharge Curves

All the measurements recorded during the galvanostatic cycling for vanadium and organic batteries are presented in the Supporting Information (Figures S1–S3). The main cell measurements show, as expected, that higher current densities require higher cell overpotentials leading to lower energy efficiency and capacity utilization (see SI). In the case of the first Vanadium system (VFB1), the cycling at the highest current density was not possible as this required so high overpotentials that the cell voltage exceeds the cut-off voltage in that condition. The analysis of the half-cells measurements conducts to the same results obtained from the main cell analysis: first, when increasing the current density, the half-cell state of charges at the end of each step are further away from their extremes values (0–100 % SOC), which means that the capacity utilization on each side of the battery is lower. Furthermore, the measurement of the individual apparent half-cells overpotentials confirms the increase on the overall overpotential of the system with the current density and allows distinguishing which side of the cell presents higher potential losses. These results are discussed in more detail below.

#### *Analysis of SOCs*

For the analysis of the half-cells state of charge we first built up the half-cells state of charge curves (*E* vs SOC) by discharging the cell to 0 % SOC followed by a charging step to 100 % SOC. To ensure the extreme SOC values, we used a potential hold in the end of the discharge and charge steps with a low current cut-off of 0.5 mA cm$^{-2}$. The construction of the *E* vs SOC curves becomes easier and faster with this measurement set-up because the half-cell potentials are recorded on-line against the reference electrodes. The experimental half-cells state of charge curves are presented on the SI and compared to the theoretical curves obtained from Nernst equation.[28] The experimental curves show a slight imbalance and the extreme SOCs were not achieved with the protocol used. However, after considering the imbalance and excluding the extreme SOCs, we obtained a high correlation. Furthermore, the VFB curves are in agreement with experimental results previously reported (see Figure S2 A and B).[19] Then, we consider that the obtained curves are suitable enough to predict the half-cell SOCs during battery operation if not considering extreme SOCs, below 5 % or above 95 %.

Figures 2 and 3 exhibit the measurements of the half-cell potentials of the positive and negative side (measurements 4 and 5 in Figure 1) during cycling at the different current densities studied, presenting the SOC achieved at the end of the charge and discharge steps for the VFB1 and organic system. The same analysis can be conducted for the second vanadium system VFB2 but it is excluded in this section. Figures 2C and 3C presents the capacity utilization on each side of the cell, calculated as the SOC difference between the end of each charge and discharge step, and compares it against the capacity utilization during discharge measured in the main cell. The strong agreement obtained confirms the reliability of the half-cells state of charge measurements of this system.

As expected, the SOCs achieved on each side of the cell are further away from their extremes when increasing the current density after every three cycles, as the higher current values lead to higher overpotentials and lower capacity utilization. This effect is clearly higher for the VFB1 that was cycled using higher current densities and suffered higher potential losses, mostly in the negative side, as confirmed in the next section. The vanadium system experienced a noticeable capacity decay after every cycle, clearly shown by the achieved SOCs in each cycle and the discharge capacity measured in the main cell (Figure 2). We attribute this to the instability of the $V^{2+}$ species that can be oxidized back to $V^{3+}$ in contact with air oxygen.[29,30] The oxidation of $V^{2+}$ causes an imbalance in the cell, with the negative side working at lower SOCs as it is shown in the half-cell measurements in Figure 2. Despite degassing the electrolyte during the whole experiment by bubbling nitrogen into the reservoirs, these results suggest that it was not enough to remove the oxygen from the system, which can also permeate through the tubing, connectors, gaskets and other cell components.[31]

During the cycling of the organic-FB, performed using lower current densities, lower overpotentials were developed. This resulted on higher capacity utilization achieving SOCs closer to the extreme values, even when increasing the current density values (Figure 3). This system showed a high capacity retention in the studied conditions, as it was expected from the previous reports of high stability of this redox couple.[26] Furthermore, we can see a slight imbalance with the positive electrolyte moving at higher SOCs than the negative electrolyte. However, the accuracy of these measurements at the extreme SOC values is lower and it strongly depends on the quality of the half-cell state of charge curves built-up beforehand. These measurements show that the on-line monitoring of the half-cells during operation can provide valuable information to get an insight into the battery performance, e. g., allowing to distinguish a cell imbalance or capacity fades on each side of the cell, becoming even more valuable when applied for long cycling processes.

Finally, the leakless Ag/AgCl reference electrodes (ET072 electrode from eDAQ) used in the reference cells, demonstrated a high reliability during these experiments of approximately 7-hour-duration without noticeable potential shifts. However, for longer cycling tests where potential shifts are likely to occur, these reference electrodes are still suitable as they can be easily removed to regenerate or be replaced.

#### *Analysis of Apparent Overpotentials*

The apparent overpotentials recorded for the three systems during cycling are presented in the Figures S1–S3 of the Supporting Information (measurements 6 and 7 for the positive and negative electrode, respectively). Table 2 summarizes the apparent overpotentials on both sides of the cell during

Research Article
doi.org/10.1002/batt.202400394
Chemistry Europe
European Chemical Societies Publishing

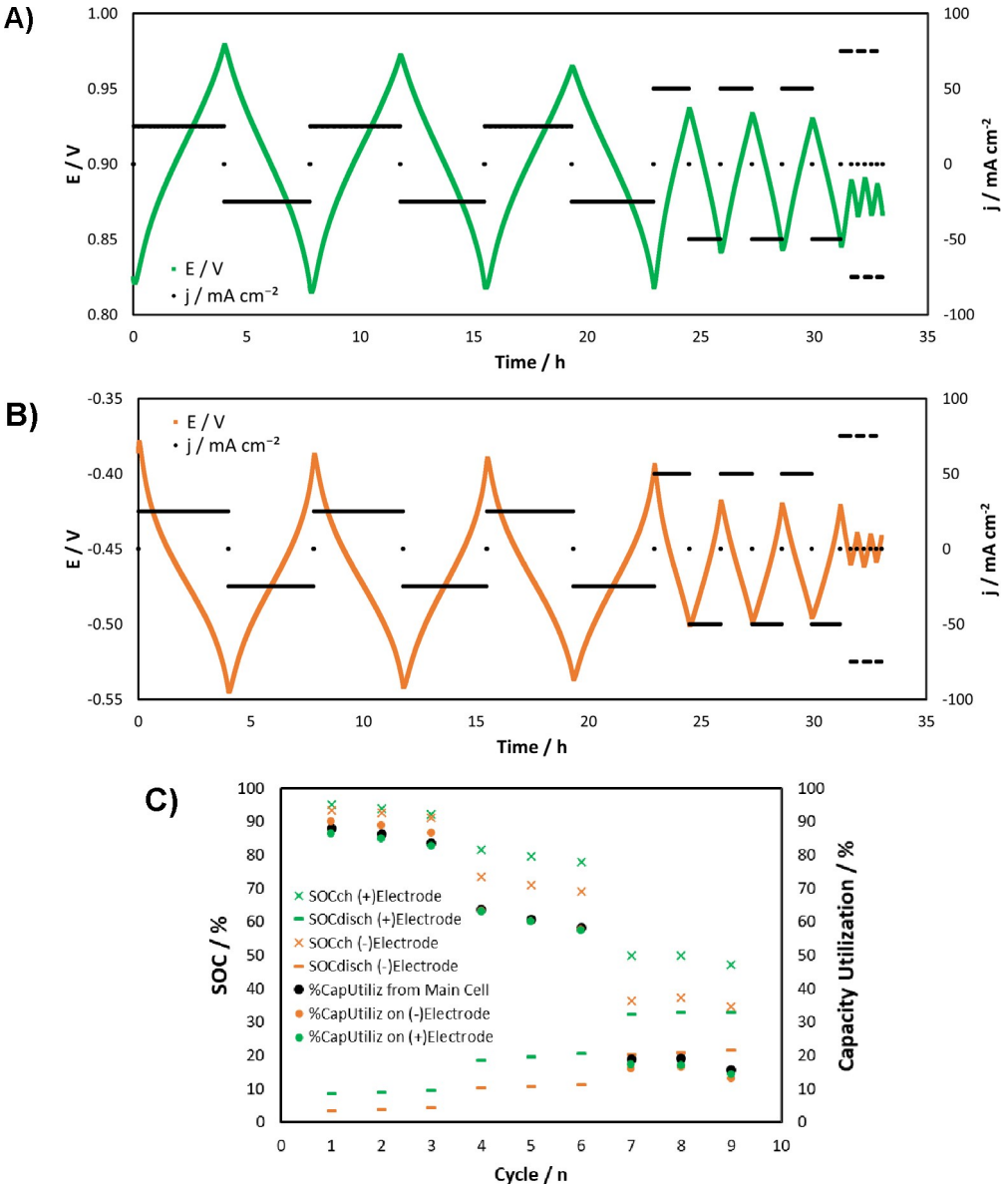


**Figure 2.** Vanadium-FB1 cycling figures, half-cell potentials and SOCs achieved. A) Positive electrode half-cell potential vs reference Ag/AgCl (measurement 4) and current density during cycling. B) Negative electrode half-cell potential vs reference Ag/AgCl (measurement 5) and current density during cycling. **C)** SOCs achieved at the end of each cycle after charge and discharge, $SOC_{ch}$ and $SOC_{disch}$, respectively, on the positive and negative electrode. Capacity utilization during discharge measured in the Main Cell and capacity utilization on each electrolyte determined as the difference between $SOC_{ch}$ and $SOC_{disch}$ for each cycle.

**Table 2.** Summary of apparent discharge overpotentials recorded with measurements 6 and 7 for positive and negative electrode, respectively. The values corresponds to the apparent overpotentials measured at 50% SOC, calculated as an average of the three cycles for each current density and considering the background potential before starting the discharge step.

| | VFB1 | | VFB2 | | OFB | | |
|---|---|---|---|---|---|---|---|
| $j$/mA cm$^{-2}$ | $\eta+$/mV | $\eta-$/mV | $\eta+$/mV | $\eta-$/mV | $j$/mA cm$^{-2}$ | $\eta+$/mV | $\eta-$/mV |
| 25 | −41 | 91 | −49 | 79 | 12.5 | [b] | 13 |
| 50 | −84 | 175 | −72 | 146 | 25 | −32 | 26 |
| 75 | −118 | 263 | −102 | 197 | 37.5 | −42 | 34 |
| 100 | [a] | [a] | −126 | 241 | 50 | −54 | 42 |

[a] Cycling of VFB1 at 100 mA cm$^{-2}$ was not performed as the cell voltage exceeds the cut-off due to the high overpotentials required. [b] Positive electrode apparent overpotentials of Organic-FB at 12.5 mA cm$^{-2}$ are not reported because the noisy measurement and short resting time do not allow determining a clear value.

Research Article
doi.org/10.1002/batt.202400394
Chemistry Europe
European Chemical Societies Publishing

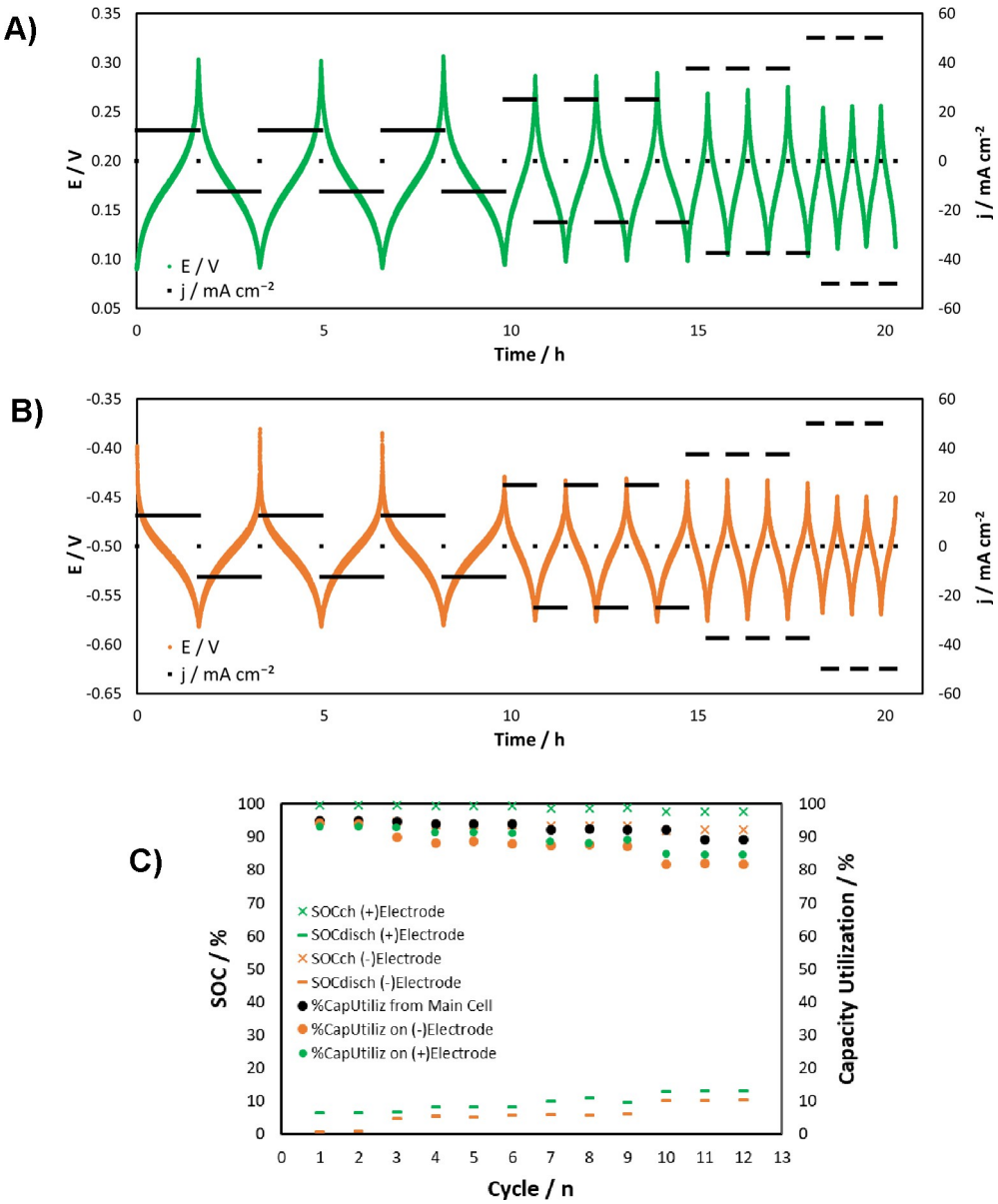


**Figure 3.** Organic-FB cycling figures, half-cell potentials and SOCs achieved. A) Positive electrode half-cell potential vs reference Ag/AgCl (measurement 4) and current density during cycling. B) Negative electrode half-cell potential vs reference Ag/AgCl (measurement 5) and current density during cycling. **C)** SOCs achieved at the end of each cycle during charge and discharge, $SOC_{ch}$ and $SOC_{disch}$, respectively, on the positive and negative electrode. Capacity utilization during discharge measured in the Main Cell and capacity utilization on each electrode determined as the difference between $SOC_{ch}$ and $SOC_{disch}$ for each cycle.

discharge at 50% SOC. Even though we can determine the electrode polarization at any time of the process, we selected the value at 50% SOC as it corresponds to steady state and it allows studying the systems at the same condition and performing a more proper analysis of the different current densities.

Table 2 clearly shows the much higher apparent overpotentials required in the VFB comparing with OFB, which is in agreement with the slow kinetics of the vanadium reactions. The vanadium rate constants for the positive and negative side, using the same electrolyte and electrode material of this work, were previously determined as $1.4\times10^{-4}$ and $2.5\times10^{-5}$ cm s$^{-1}$, respectively.[32] Furthermore, the half-cells apparent overpotentials measured on each side of the vanadium cell confirms that the negative side is responsible of most of the potential losses due to the slow kinetics of the $V^{2+}/V^{3+}$ couple.[22,24] For both Vanadium-FBs, the contribution of the negative side for the overall electrode overpotential remains at 66–69% at the studied current densities. Finally, the comparison of both vanadium systems shows that the VFB1 suffers from higher apparent overpotentials on both sides of the cell, mainly on the negative side, which confirms the lower performance of that system and the limitation to operate at higher current densities. We attribute the difference on the electrodes behavior to the activity of the carbon electrodes towards the vanadium reactions, which arises from the different felt composition and

the activation treatment. These results emphasize the importance of a proper electrode pre-treatment to achieve high FB performance. We did not perform further analysis of the felts as it is out of the scope of this work.

In the case of the Organic-FB, the overall electrode overpotential is equally distributed on both sides of the battery with a slightly higher contribution of the positive side (Table 2). For the four current densities studied, the contribution ratio of the positive side overpotential to the overall electrode overpotential during discharge is around 52–56%. These results are coherent if we consider that the oxidation rate constant of BTMAP-Fc is slightly lower than the reduction rate constant of BTMAP-Vi, which were calculated in a previous work using rotating disc electrode measurements[26] ($1.4\times10^{-2}$ and $2.2\times10^{-2}$ cm s$^{-1}$, respectively).

Furthermore, the recording of the apparent overpotentials shows which side of the battery is the limiting side during cycling. This can be seen at the end of each step, where the apparent overpotential increases rapidly on the limiting side of the cell due to mass transport limitations. These results are coherent with the half-cells SOCs measurements when revealing the limiting side of the battery and confirm the reliability of the measurements recorded with the experimental set-up.

### *Membrane Potential Measurements*

The membrane potentials recorded with this experimental set-up (Measurement 8) show a low contribution of the potential drop through the membrane to the overall cell voltage. These values correspond to 16 mV for both VFBs and 30 mV for the OFB when there is no current flow on the cell. In a previous work,[33] Kumbur referred to the potential difference across the membrane as the Donnan potential, presenting it as a result of the proton concentration difference between the two electrolytes. The membrane potential drop contribution on a vanadium flow cell was calculated as around 30 mV, which is a reasonable agreement with the values measured in this work.

The measured membrane potentials exhibit a slight change when there is an applied current on the system, which increases proportionally with the current density. This fact suggests the presence of a small parasitic current flowing through the OCV-cell after the main cell. However, as the membrane-drop measurements during cycling show, the deviations are in the order of 20, 5 and 30 mV for the highest current densities tested for VFB1, VFB2 and OFB, respectively. We understand the importance of recognizing them using the membrane potential measurement. However, we think that the slight deviations should not affect the main results and discussion presented in this work.

### *Analysis of OCV Measurements (Before and After Main Cell)*

The OCV measurements allow estimating the state of charge of the full cell, but they do not provide complete information in case of imbalance. In that situation, the limiting side of the battery would determine the cell SOC. In this work, by recording the OCV before and after the main cell, we aimed to measure the cell-conversion during battery operation. Figure 4 presents the OCV measurements before and after the main cell during the cycling of the VFB1, clearly showing the conversion through the cell.

However, the high flow rate and low conversion in one-step for the applied current densities do not allow doing an accurate analysis of the achieved conversion. We conclude that this analysis is better suited for cell-stacks or larger systems with higher conversion rate in one-step.

### Polarization Curves

Polarization curves provide an approach to distinguish the potential losses occurring in a cell. In this work, we demonstrate that the measurement of the individual apparent overpotentials strongly improves the analysis of these curves as it allows studying the distribution of the potential losses between the two electrodes. Furthermore, compared with previous works,[19,23] the on-line overpotential measurement enables to conduct the study of these curves in a simpler and faster way using the standard slope approach.

The results presented in this section correspond to the recordings from the slope approach. We use the galvanostatic-step method to compare and validate those measurements. All the polarization curves as well as the comparison of both methods are presented in the SI. The results show a high

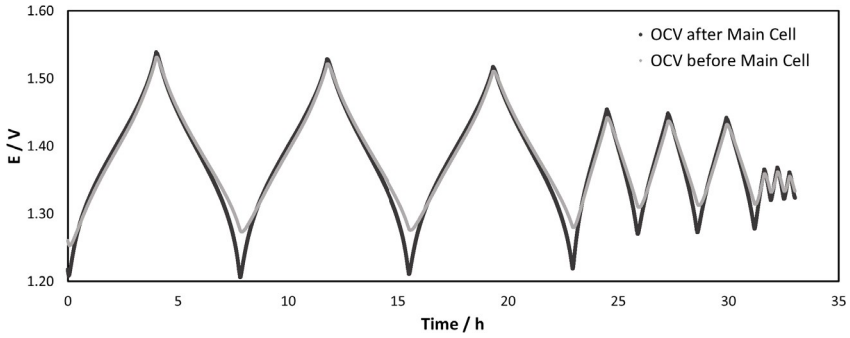


**Figure 4.** OCV measurements in OCV-cells before and after the main cell for VFB1 (measurements 2 and 3).

Research Article
doi.org/10.1002/batt.202400394
Chemistry Europe
European Chemical Societies Publishing

agreement between the two approaches in most of the studied conditions. The exceptions appear at the end of the polarization curves for the lowest SOC and flow rate (20 SOC–20 mL min$^{-1}$), where the mass transfer limitations increase rapidly because exhaustion of the electrolyte. At those conditions, the step approach lacks of sufficient accuracy and it becomes challenging to define a steady voltage value for the high current density region. In this section, we analyze the recorded apparent overpotentials on the positive and negative side during the discharge polarization curves measurements. Figures 5 and 6 show the apparent overpotentials for VFB1 and OFB, respectively, at different SOCs and flow rates.

The first point to consider about the VFB results (Figure 5) is that the apparent overpotentials on the negative electrode are higher than on the positive side in all the studied conditions, which agrees with the lower kinetics of the $V^{2+}/V^{3+}$ couple already discussed in this article. Apparent overpotentials can be utilized to construct Tafel plots and calculate apparent exchange current densities. This analysis is presented in the Supporting Information, but this results in underestimation of the exchange current densities. Correct values could be obtained with the system able to measure real overpotentials

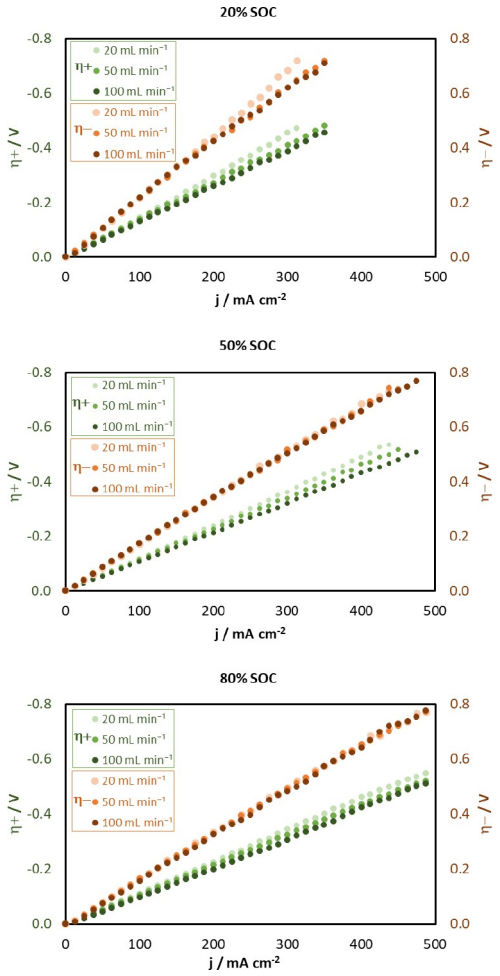


**Figure 5.** Half-cells apparent overpotentials of VFB1 measured during polarization curves at different SOCs (20, 50 and 80 %) and flow rates (20, 50 and 100 mL min$^{-1}$).

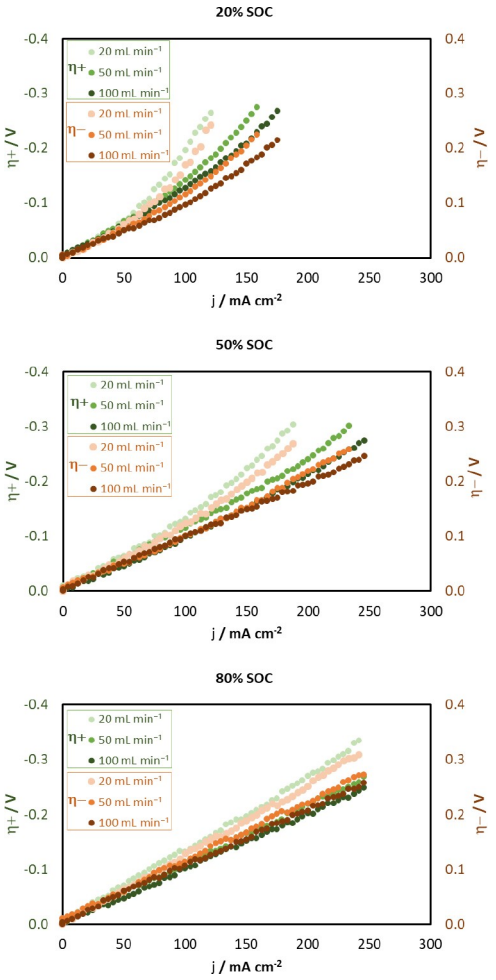


**Figure 6.** Half-cells apparent overpotentials of Organic-FB measured during polarization curves at different SOCs (20, 50 and 80 %) and flow rates (20, 50 and 100 mL min$^{-1}$).

without *iR* drop between the electrodes. Secondly, all the VFB curves have a linear trend indicating that the biggest contribution to potential losses arises from ohmic drop, as it has been previously reported for these systems.[21] Furthermore, the curves are characterized by the lack of charge transfer polarization on the low current density region. This is attributable to the use of porous carbon electrodes with high surface area[21] and the electrode pre-treatment that enhances the activity towards vanadium reactions. Regarding the high current density region, related with the mass transfer polarization, the curves do not show appreciable potential losses attributable to starvation of the reacting species. However, slight mass transfer limitations are visible in the curves corresponding to 20 % SOC–20 mL min$^{-1}$ exhibiting a small deviation from the linear trend as the current density is increasing. Roth et al. reported that the overpotentials are not dependent of the SOCs,[23] and then the linear increase (or decrease) remains constant at different SOCs in absence of starvation effects. However, our results show a small increase on the slope at lower SOCs. We believe that mass transfer effects are responsible of that slight resistance increase because of the lower amount of reacting species. Finally, the

Research Article
doi.org/10.1002/batt.202400394


positive electrode polarization increases at a faster rate with the current density at lower flow rates, while the negative electrode slope remains constant (except the 20% SOC–20 mL min$^{-1}$). We also attribute that effect to mass transfer limitations because of the higher viscosity of the positive electrolyte.[19]

The overpotentials distribution on the organic-FB (Figure 6), show a similar contribution from both sides with slightly higher polarization of the positive electrode, in agreement with the cycling experiments. Similar to the VFB1, a flow rate reduction results on higher electrode polarization due to higher mass transfer effects. In this case, the curves clearly exhibit starvation effects, mainly at the lower SOCs, leading to much lower limiting current densities. We attribute this to the lower concentration of this system (0.4 M). This assumption is supported by the linear trend of the 80%SOC curves, where the concentration of the reacting species is higher.

The results presented in this section clearly evidences how this experimental set-up enables a deeper study of the polarization curves using a simple and fast approach. By confirming previous results of VFBs, we demonstrated how the on-line monitoring of the individual apparent overpotentials allows distinguishing the contribution of each electrode to the overall cell polarization with high reliability.

### Measurements Validation

The voltage of the main cell can be calculated considering the open circuit voltage and the potential losses (overpotentials) occurring in the cell during operation. Using the half-cell open circuit potentials and apparent overpotentials we obtain:

$$E_{main\ cell} = E^{+}_{OCP} - E^{-}_{OCP} + \eta^{+} - \eta^{-} + E_{memb}$$

Where

$E^{+}_{OCP}$ is the positive electrode open circuit half-cell potential (measurement 4),

$E^{-}_{OCP}$ is the negative electrode open circuit half-cell potential (measurement 5),

$\eta^{+}$ is the positive electrode apparent overpotential (measurement 6),

$\eta^{-}$ is the negative electrode apparent overpotential (measurement 7),

$E_{memb}$ is the potential drop through the membrane (measurement 8).

As the experimental set-up allows recording all these parameters, we can validate the system by comparing the cell voltage measured in the main cell with the calculated one. The cycling figures for the three studied systems show the excellent agreement between the measured and calculated values. Figure 7A and B show the validation of the results for the VFB1,

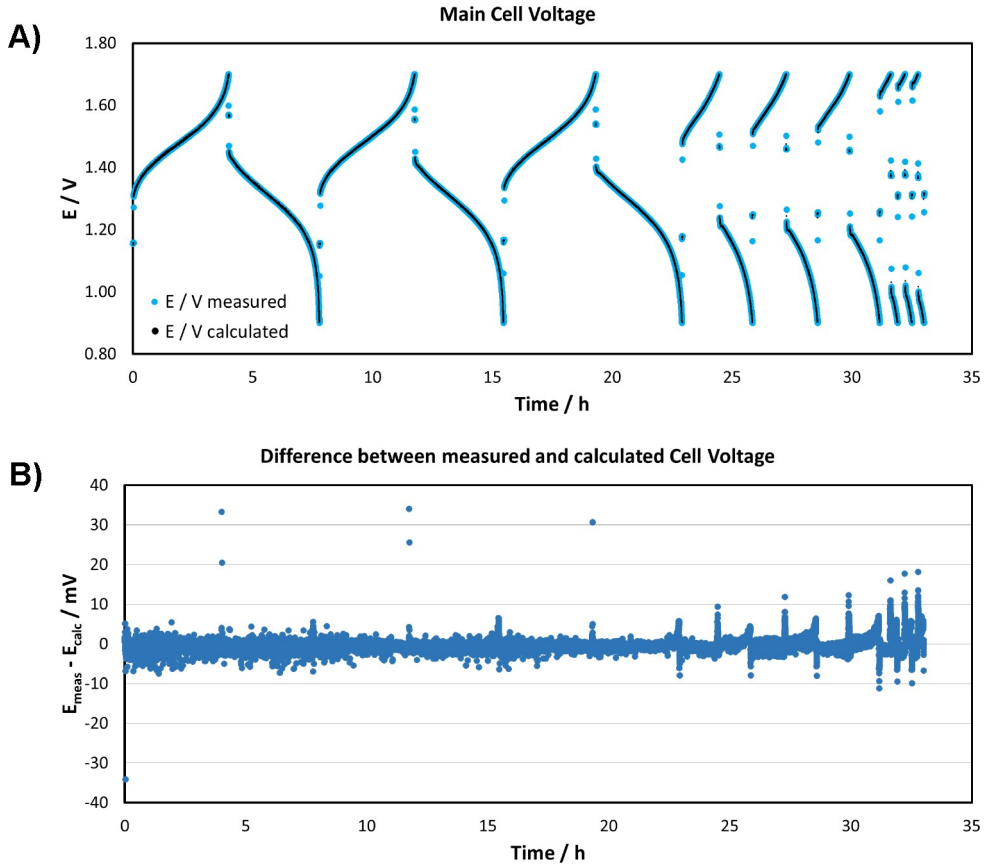


**Figure 7.** A) Comparison of the recorded main cell voltage values against the calculated values during the cycling experiments of the VFB1. B) Difference between the measured ($E_{meas}$) and calculated ($E_{calc}$) cell voltage.

while the VFB2 and Organic-FB curves are presented in the Supporting Information S5. For all the systems, the difference is lower than 10 mV for most of the cycling test, with some points exceeding that value at the end of the charge or discharge step where the electrodes polarization present a sudden increase. These results strongly validates the reliability of the experimental set-up presented in this work.

Ideally, the potential difference between the two reference electrodes ($E_{memb}$) should not change when the current is turned on and off. This indicates that there is some shunt current passing through the cell. To evaluate this, impedance between all parts was evaluated for VFB1 and the system was analyzed by Kirchoffs laws. Based on this analysis, the resistance between electrodes 6 and 7 are ca. 1300 Ω, and ca. 0.006 % of the current flows through OCV-cells as shunt currents. Although this current is small, it is sufficient to generate significant *iR* drop for apparent overpotential measurements. As the equation above is able to match the experimental values with high accuracy, this confirms that Ohmic losses of the main cell are included in the measurements of overpotentials and the potential difference across the membrane. For measuring real overpotentials, membrane in OCV-cell after the main cell can be replaced by Teflon sheet to make sure that no current is flowing between electrodes in measurements 6 and 7. This is demonstrated in the Supporting Information S7 and S8.

## Conclusions

In the present work, we demonstrated that the measurement system provides a reliable and strong monitoring of the FB performance during operation. The validation of the measurements shows a high agreement of the calculated values compared with main cell measurements, which confirms the high reliability of the system. Using this approach, we confirmed previous results obtained for vanadium-FB and demonstrated its applicability to further systems. We showed how the on-line measurements of half-cell potentials and apparent overpotentials allow a deeper study of the cell using a simple and fast approach.

- The half-cell open circuit potential measurements provide valuable information about the processes occurring into the cell and allows distinguishing the origin of capacity fades or imbalances. It is important to remark that the reliability of the measurements highly depend on the build of the *E* vs SOC curve made beforehand. In this case, we obtained a suitable agreement with the theoretical curves after correction of the systems imbalance. In the future, in order to avoid differences due to possible imbalances, the experimental curves could be improved by building them for each side separately using a non-limiting side.
- We also demonstrated the powerful information obtained from the individual apparent overpotential measurements. The on-line time-dependent measurements of apparent overpotentials on both electrodes allows recognizing the origin of the potential losses during operation. An alternative to measure the real overpotentials is also presented. These measurements provide a valuable information for the study and improvement of batteries' performances.
- The conversion through the cell using the OCV measurements (before and after the cell) was not possible due to the low current densities. That study could be applied for larger systems with higher conversion in one-step. Then, the measurement system for lab-scale usage can be simplified to just one cell including the reference electrodes after the main battery.

## Supporting Information Summary

The authors have cited additional references within the Supporting Information (Ref. [34]).

## *Acknowledgements*

We would like to acknowledge the funding received from the European Union's Horizon2020 Research and Innovation programme under grant agreement No 875565 (Project CompBat). G.G. gratefully acknowledges the financial support from the University of Turku Graduate School. P.P. gratefully acknowledges the Academy Research Fellow funding (grant no. 315739, 343791, 320071, and 343794) from Research Council Finland, and European Research Council through a Starting grant (agreement no. 950038). Materials Analysis and Research Infrastructure (MARI) of the University of Turku was utilized in this work. We acknowledge the work conducted by Ali Tuna on the exploration of the synthesis of BTMAP-Fc.

## *Conflict of Interests*

The authors declare no conflict of interest.

## *Data Availability Statement*

The data that support the findings of this study are available in the supplementary material of this article.

**Keywords:** Flow battery · Half-cells measurements · On-line monitoring · State of charge · Overpotential

[1] P. Alotto, M. Guarnieri, F. Moro, *Renew. Sust. Energy Rev.* **2014**, *29*, 325–335.
[2] J. Girschik, L. Kopietz, M. Joemann, A. Grevé, C. Doetsch, *Chem. Ing. Tech.* **2021**, *93*, 523–533.
[3] G. Kear, A. A. Shah, F. C. Walsh, *Int. J. Energy Res.* **2012**, *36*, 1105–1120.
[4] E. Sánchez-Díez, E. Ventosa, M. Guarnieri, A. Trovò, C. Flox, R. Marcilla, F. Soavi, P. Mazur, E. Aranzabe, R. Ferret, *J. Power Sources* **2021**, *481*, 228804.
[5] V. Singh, S. Kim, J. Kang, H. R. Byon, *Nano Res.* **2019**, *12*, 1988–2001.
[6] T. Jirabovornwisut, A. Arpornwichanop, *Int. J. Hydrogen Energy* **2019**, *44*, 24485–24509.
[7] D. G. Kwabi, Y. Ji, M. J. Aziz, *Chem. Rev.* **2020**, *120*, 6467–6489.

[8] Y. Liu, Q. Chen, X. Zhang, J. Ran, X. Han, Z. Yang, T. Xu, *Curr. Opin. Electrochem.* **2022**, *32*, 100895.
[9] F. Zhu, W. Guo, Y. Fu, *Chem. Asian J.* **2023**, *18*, e202201098.
[10] Z. Li, T. Jiang, M. Ali, C. Wu, W. Chen, *Energy Storage Mater.* **2022**, *50*, 105–138.
[11] Y. Yang, Y. Zhang, L. Tang, T. Liu, S. Peng, X. Yang, *J. Power Sources* **2020**, *450*, 227675.
[12] D. Reynard, H. Vrubel, C. R. Dennison, A. Battistel, H. Girault, *ChemSusChem* **2019**, *12*, 1222–1228.
[13] O. Nolte, I. A. Volodin, C. Stolze, M. D. Hager, U. S. Schubert, *Mater. Horiz.* **2021**, *8*, 1866–1925.
[14] M. Skyllas-Kazacos, M. Kazacos, *J. Power Sources* **2011**, *196*, 8822–8827.
[15] S. Ressel, F. Bill, L. Holtz, N. Janshen, A. Chica, T. Flower, C. Weidlich, T. Struckmann, *J. Power Sources* **2018**, *378*, 776–783.
[16] T. Haisch, H. Ji, C. Weidlich, *Electrochim. Acta* **2020**, *336*, 135573.
[17] J. Grosse Austing, C. Nunes Kirchner, E. M. Hammer, L. Komsiyska, G. Wittstock, *J. Power Sources* **2015**, *273*, 1163–1170.
[18] C. Choi, Y. Choi, S. Kim, H. Jung, H. T. Kim, *Electrochim. Acta* **2016**, *213*, 490–495.
[19] M. Cecchetti, A. Casalegno, M. Zago, *J. Power Sources* **2018**, *400*, 218–224.
[20] A. Bourke, D. Oboroceanu, N. Quill, C. Lenihan, M. A. Safi, M. A. Miller, R. F. Savinell, J. S. Wainright, V. SasikumarSP, M. Rybalchenko, P. Amini, N. Dalton, R. P. Lynch, D. N. Buckley, *J. Electrochem. Soc.* **2023**, *170*, 030504.
[21] D. Aaron, Z. Tang, A. B. Papandrew, T. A. Zawodzinski, *J. Appl. Electrochem.* **2011**, *41*, 1175–1182.
[22] C. N. Sun, F. M. Delnick, D. S. Aaron, A. B. Papandrew, M. M. Mench, T. A. Zawodzinski, *ECS Electrochem. Lett.* **2013**, *2*, A43–A45.
[23] J. Langner, J. Melke, H. Ehrenberg, C. Roth, *ECS Trans.* **2014**, *58*, 1–7.
[24] D. Aaron, C. N. Sun, M. Bright, A. B. Papandrew, M. M. Mench, T. A. Zawodzinski, *ECS Electrochem. Lett.* **2013**, *2*, A29–A31.
[25] J. Piwek, G. Gonzalez, P. Peljo, E. Frackowiak, *Carbon* **2023**, *215*, 118483.
[26] E. S. Beh, D. De Porcellinis, R. L. Gracia, K. T. Xia, R. G. Gordon, M. J. Aziz, *ACS Energy Lett.* **2017**, *2*, 639–644.
[27] P. C. Ghimire, A. Bhattarai, T. M. Lim, N. Wai, *Batteries* **2021**, *7*, 53.
[28] M. Ciobanu, J. P. Wilburn, M. L. Krim, D. E. Cliffel, in *Handbook of Electrochemistry*, Elsevier **2007**, pp. 3–29.
[29] K. Ngamsai, A. Arpornwichanop, *J. Power Sources* **2015**, *295*, 292–298.
[30] N. H. Choi, S. Kwon, H. Kim, *J. Electrochem. Soc.* **2013**, *160*, A973–A979.
[31] N. Poli, M. Schäffer, A. Trovò, J. Noack, M. Guarnieri, P. Fischer, *Chem. Eng. J.* **2021**, *405*, 126583.
[32] I. Kroner, M. Becker, T. Turek, *ChemElectroChem* **2020**, *7*, 4314–4325.
[33] K. W. Knehr, E. C. Kumbur, *Electrochem. Commun.* **2011**, *13*, 342–345.
[34] M. Skyllas-Kazacos, L. Cao, M. Kazacos, N. Ausar, A. Ousa, *ChemSusChem* **2016**, *9*, 1521–1543.

Manuscript received: June 19, 2024
Revised manuscript received: September 18, 2024
Accepted manuscript online: October 8, 2024
Version of record online: November 14, 2024